RESEARCH ARTICLE

INTERNATIONAL RESEARCH JOURNAL OF MULTIDISCIPLINARY TECHNOVATION

Asian Research Association

DOI: 10.54392/irjmt2652

Composition-Dependent Magnetic Reversal and Partial Exchange Coupling in $SrFe_{12}O_{19}$/FeCo Nanocomposites

R. Akshaya [a], B. Gokul [a, *]

[a] Department of Physics, Kongunadu Arts and Science College, Coimbatore-641029, Tamil Nadu, India.

* Corresponding Author Email: gokulbangaru@gmail.com

DOI: https://doi.org/10.54392/irjmt2652

Received: 30-06-2026; Revised: 10-08-2026; Accepted: 17-08-2026; Published: 31-08-2026

Abstract: $SrFe_{12}O_{19}$/FeCo hard–soft magnetic nanocomposites with different hard-to-soft magnetic phase ratios were successfully synthesized using a combination of sol–gel autocombustion and wet-chemical methods, followed by physical mixing. X-ray diffraction analysis confirmed the formation and coexistence of the hexagonal $SrFe_{12}O_{19}$ hard magnetic phase and body-centred cubic FeCo soft magnetic phase, with no detectable crystalline impurity phases. The structural parameters showed a composition-dependent variation in crystallite size and lattice strain, indicating changes in crystallinity and structural distortion with FeCo incorporation. The magnetic properties exhibited a strong dependence on the hard–soft phase ratio. With increasing FeCo content, the coercivity decreased from 1795 to 866 Oe, which can be attributed to the increasing contribution of the magnetically soft FeCo phase and its easier magnetization reversal. The differential magnetization (dM/dH) curves displayed a dominant central switching peak accompanied by symmetric secondary features, suggesting the coexistence of different magnetization-reversal processes and supporting the presence of partial exchange coupling between the hard and soft magnetic phases. Furthermore, the effective magnetic anisotropy decreased with increasing FeCo content due to the reduced relative contribution of the high-anisotropy $SrFe_{12}O_{19}$ phase. Despite the decrease in coercivity, the maximum energy product increased from 0.09 to 0.18 MGOe, demonstrating that appropriate adjustment of the hard-to-soft phase ratio can improve the overall magnetic performance. These findings demonstrate that FeCo incorporation provides an effective approach for balancing saturation magnetization and coercivity, highlighting the potential of $SrFe_{12}O_{19}$/FeCo nanocomposites as rare-earth-free materials for permanent magnet applications.

Keywords: Permanent Magnets, Partial Exchanged-Coupled, Sol-Gel Autocombustion, Physical Mixing, Maximum Energy Product

1. Introduction

In this modern world there will be big incentive to develop permanent magnets. And these permanent magnets are utilized every year as key components in electrical generators, motors, magnetrons, hard disk drives, and loudspeakers. Furthermore, permanent magnets are essential for the development of innovative wind turbines, energy harvesters, magnetic freezers, Flywheel energy storage systems, and electric vehicles [1].

Ferrites based magnets are the most significant magnetic materials due to their chemical stability, low cost and a wide range of technological applications [2]. Ferrite nanocomposites have gained attention recently because of the magnetic connection between these two phases, which influences the composite materials microstructural and magnetic characteristics such as coercivity, remanence magnetization, and saturation magnetization. The technological significance of these nanocomposite magnetic materials is very significant to achieve maximum energy product B-H (max). Several research teams have tried doping various magnetic, non-magnetic, and rare-earth elements to improve the magnetic characteristics of M-type hexaferrite, but they haven't been able to boost coercivity without lowering magnetization. So, the alternative method is developed to increase coercivity without decreasing the magnetization by combining one soft magnetic material and one hard magnetic material with the name of exchange coupled magnet [3, 4]. Unlike ordinary single-phase magnets, magnetically exchanged coupled magnets have both hard and soft magnets. When the spins of the hard and soft phases interact magnetically on the nanoscale, the two-phase magnet behaves like a strong magnet [5]. Here, hexaferrites are the most important hard magnetic material that used in several application. On the other hand, soft magnets such as metals like Fe, Co and ferrites like Fe_2O_3, $MnFe_2O_4$, etc are used widely [6].

To enhance the magnetic property to achieve maximum energy product by the interaction of hard magnetic material and soft magnetic material. The most important property for permanent magnet is coercivity that it has ability to retain their magnetization. For this, ferrites are the best one because of their uniaxial magneto crystalline anisotropy. These ferrites are significantly cost effective to produce and it can maintain their magnetic property at high temperature and also have high resistance to corrosion. For this property ferrites are used widely in industrial motor applications. However, in practical nanocomposites, complete exchange coupling is rarely achieved due to structural imperfections such as grain growth, particle agglomeration, interfacial defects, strain, and non-uniform phase distribution. Under such conditions, only a portion of the soft magnetic phase interacts effectively with the hard phase, while the remaining soft regions reverse independently. This intermediate magnetic behaviour is partial exchange coupling.

Partial exchange coupling is commonly identified using magnetic characterization techniques such as hysteresis loop analysis, derivative magnetization curves (dM/dH), and switching field distribution studies. In hysteresis loop measurements, systems with partial exchange coupling usually display a smooth magnetization curve with small kinks or subtle shoulders. These features suggest the presence of both exchange-coupled and decoupled magnetic reversal processes occurring simultaneously within the composite material [7, 8]. One of the best ferrites among all is strontium hexaferrite ($SrFe_{12}O_{19}$) due to its high coercivity, high resistance to corrosion and have good chemical stability, high curie temperature when compared to other metallic magnets. And, it is cost efficient to prepare. This hard magnetic material achieved by various methods like solid state reaction [9, 5], Sol-gel [6, 9], co-precipitation [10, 11], ball milling [12, 13], microemulsion [14, 15], aerosol [16, 17], combustion method [18], hydrothermal method [19].

Various ferrites-based composites are successfully synthesized and achieved maximum energy product. Here, strontium ferrite ($SrFe_{12}O_{19}$) is prepared by sol-gel auto-combustion. Sol-gel auto combustion is a highly efficient technique and versatile method to produce magnetic materials. This method has ability to produce chemically homogeneous and single-phase nanocomposites. It combines the homogeneity of the tradition sol-gel process with the energy efficiency of self-sustaining combustion. Iron Cobalt (FeCo) alloys are well known for their higher magnetization and it allows the material to carry higher magnetic flux density before its reaching their limit. It is easily magnetized and demagnetized with minimal energy loss with quick respond to the external magnetic field. Here, the FeCo were prepared by wet chemical method. Once the material is prepared separately, they can be mixed physically for different ratios.

In this paper, the nanocomposite material of prepared $SrFe_{12}O_{19}$/FeCo analysed by X-Ray Diffraction method (XRD) to determine structural properties, morphological studies by Field Emission Transmission Electron Microscope (FESEM), Crystallographic structure by High-resolution transmission electron microscopy (HRTEM) and most important magnetic property to determine maximum energy product of a material , enhancement of the ratio of remanence to saturation magnetization (M_r/M_s) and the demagnetization (dM/dH) curves of the nanocomposites with different ratios of hard/soft phases prove the existence of strong interaction between the nanoparticles of the hard and soft phases. And maximum energy product of $SrFe_{12}O_{19}$/FeCo are calculated.

2. Materials and Method

Nanocomposite material of hard and soft magnetic material is prepared by Sol-Gel autocombustion method and wet chemical process respectively in figure 1. The materials used in the synthesis are Strontium nitrate $Sr(NO_3)_2$, Iron (III) nitrate nonahydrate $Fe(NO_3)_3.9H_2O$, citric acid anhydrous ($C_6H_8O_7$), Ammonia solution (NH_4), Cobalt (II) nitrate hexahydrate $Co(NO_3)_2$. 6H2O, Iron (III) chloride ($FeCl_3$), Sodium Hydroxide (NaOH), Hydrazine hydrate $N_2H_4.H_2O$, Ethanol (C_2H_6O) are the materials obtained from thermo fisher, Merck, Sigma Aldrich are used without further purification.

2.1 Preparation of Hard Magnetic Material

$SrFe_{12}O_{19}$ nanoparticles are synthesized by sol-gel autocombustion method in figure 1a. 1M of is $Sr(NO_3)_2$ dissolved in 100ml of deionized water and kept in magnetic stirrer for stirring. Few minutes later, Fe $(NO_3)_3.9H_2O$ and (C_6H8O_7) is added to the above solution. After that, NH3 is added drop by drop to maintain pH 7 level. Then the solution is heated to 80˚C for 30 minutes. Again the temperature of the solution is slightly raised to 230˚C. And, the solution is subsequently heated until the combustion takes place. Finally, the burnt powders were grained and calcinated at 900˚C for 2h.

2.2 Preparation of Soft Magnetic Material

FeCo nanoparticles are synthesized by wet chemical process in figure 1b. 0.07M of $Co(NO_3)_2$ and 0.07M $FeCl_3$ molar ratio of (1:1) are taken in 30ml of deionized water and 20ml of C_2H_6O. 5G of NaOH is added to the above solution with 20ml of $N_2H_4.H_2O$ (reducing agent). The mixed solution is kept in magnetic stirrer for stirring with temperature 76˚C. The entire process is done under argon gas for 3h. After 3h, the reaction results in black precipitate and it should be

separated by washing with deionized water and ethanol using centrifuge for 3 times to get pure FeCo particles. Finally, magnetic powders were dried at hot air oven at 100˚C for 2h.

2.3 Hard/Soft Magnetic Nanocomposite

The prepared Strontium ferrite ($SrFe_{12}O_{19}$) and Iron cobalt (FeCo) nanoparticles were mixed for different ratios as hard /soft magnetic material in figure 1c. i.e., $SrFe_{12}O_{19}$/FeCo S8F2 (80:20), S7F3 (70:30), S6F4 (60:40), S5F5 (50:50) respectively. These powders were mixed and grained in the mortar for 20 mins. The mixed nanoparticles were characterized by the following studies.

2.4 Characterization

The phase structure of nanocomposite was identified using Bruker D8 Advance diffractometer evolved with CuKα (λ = 1.5406 Å) radiation operated at 40 kV and 30 mA (step size of 0.02).

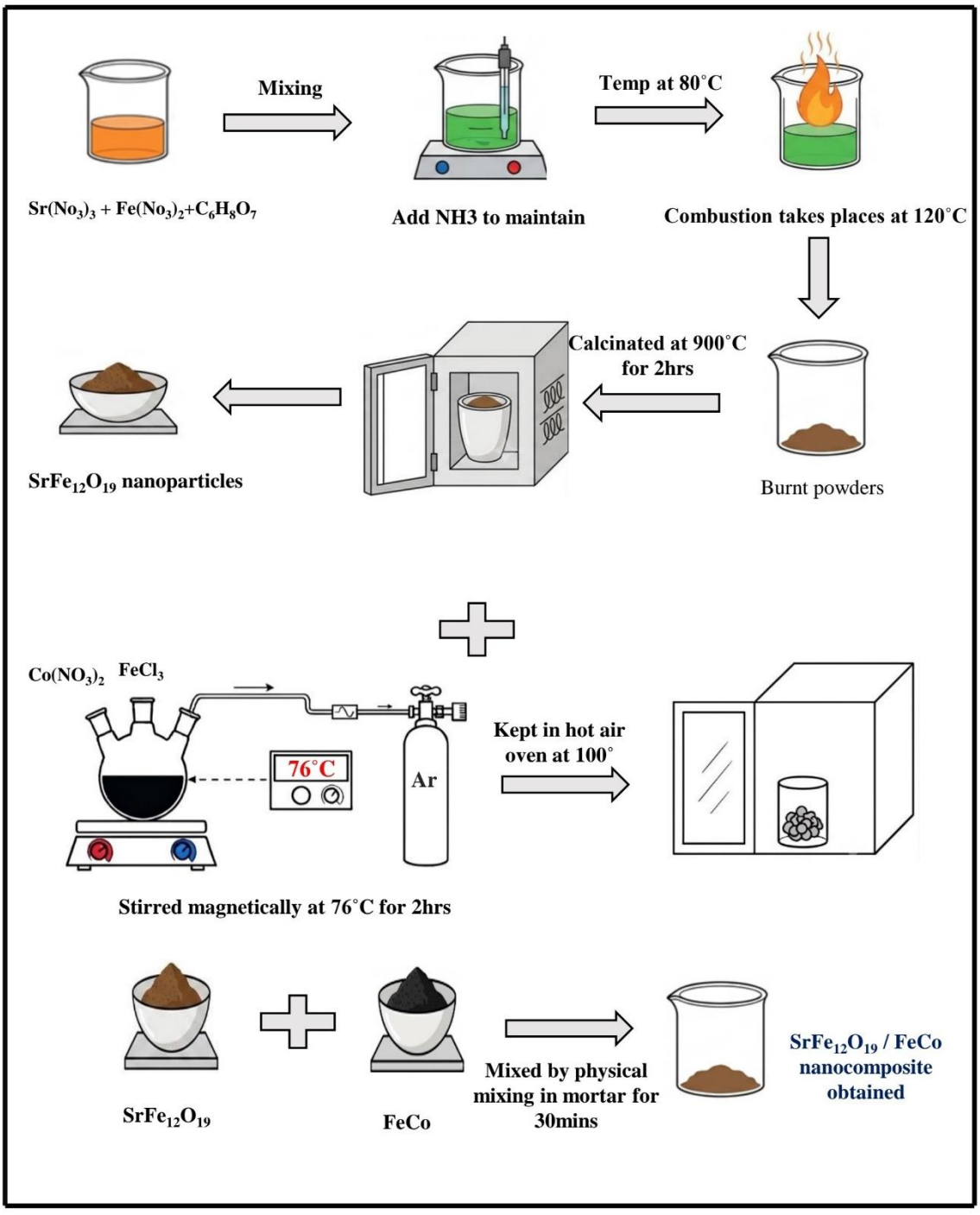

Figure 1. (a) Schematic diagram by Sol-gel autocombustion for $SrFe_{12}O_{19}$ nanoparticles, **(b)** Schematic diagram by Wet chemical method for FeCo nanoparticles, **(c)** Physical mixing process for 4 ratios.

The morphology and composition of the nanocomposites were examined using field emission scanning electron microscope (FESEM ZEISS) and energy-dispersive spectroscopy with 15 kV voltage, respectively. The shape and size of the calcinated nanocomposite powder was observed by a high-resolution transmission electron microscopy (HRTEM JEOL 2010). The magnetic hysteresis loops were measured at room temperature with maximum applied magnetic field of 20 KOe identified by Vibrating sample magnetometer Make: Lakeshore, Model: 7400 series. Saturation magnetization (Ms), remanence magnetization (Mr), the coercive field (Hc) and switching field distribution were calculated from the M-H loops.

3. Results and Discussion

3.1 Structural Properties

Figure 2 shows the XRD pattern of $SrFe_{12}O_{19}$/FeCo nanocomposite by physical mixing for 4 different ratios i.e., $SrFe_{12}O_{19}$/FeCo. The XRD patterns confirm the formation of hard/soft composite of 4 ratios with well indexed hard phase of M-type hexaferrite JCPDS card 79-1411 and soft phase with BCC Structure JCPDS card 48-1816 respectively. The peaks perfectly shows the occurrence of both hard/soft phase nanocomposites without any impurity. The M-type strontium hexaferrite with the space group of P63/mmc and FeCo with the space group of Pm-3m. These diffraction peak and high intensity of $SrFe_{12}O_{19}$ (008), (107), (201), (203), (205), (206), (217), (2011), (220) and (110) of FeCo by physical mixing results in good crystallinity of $SrFe_{12}O_{19}$/FeCo nanocomposite. The crystallite size of hard phase, soft phase are calculated using Scherrer's formula and are listed in Table 1. Scherrer formula,

$$D = \frac{k\lambda}{\beta cos\theta} \quad (1)$$

Where, d is the crystallite size, k is the shape factor, λ = 1.5406Å is the x-ray wavelength, β is the line broadening at half the maximum intensity (FWHM) in radians, and θ is the Bragg's angle. The structural parameters like lattice constant (a) and (b), average crystalline size D (nm), Strain (ε), are calculated from the diffraction peaks and listed in Table 1. The microstrain were estimated by,

$$\varepsilon = \frac{\beta}{4tan\theta} \quad (2)$$

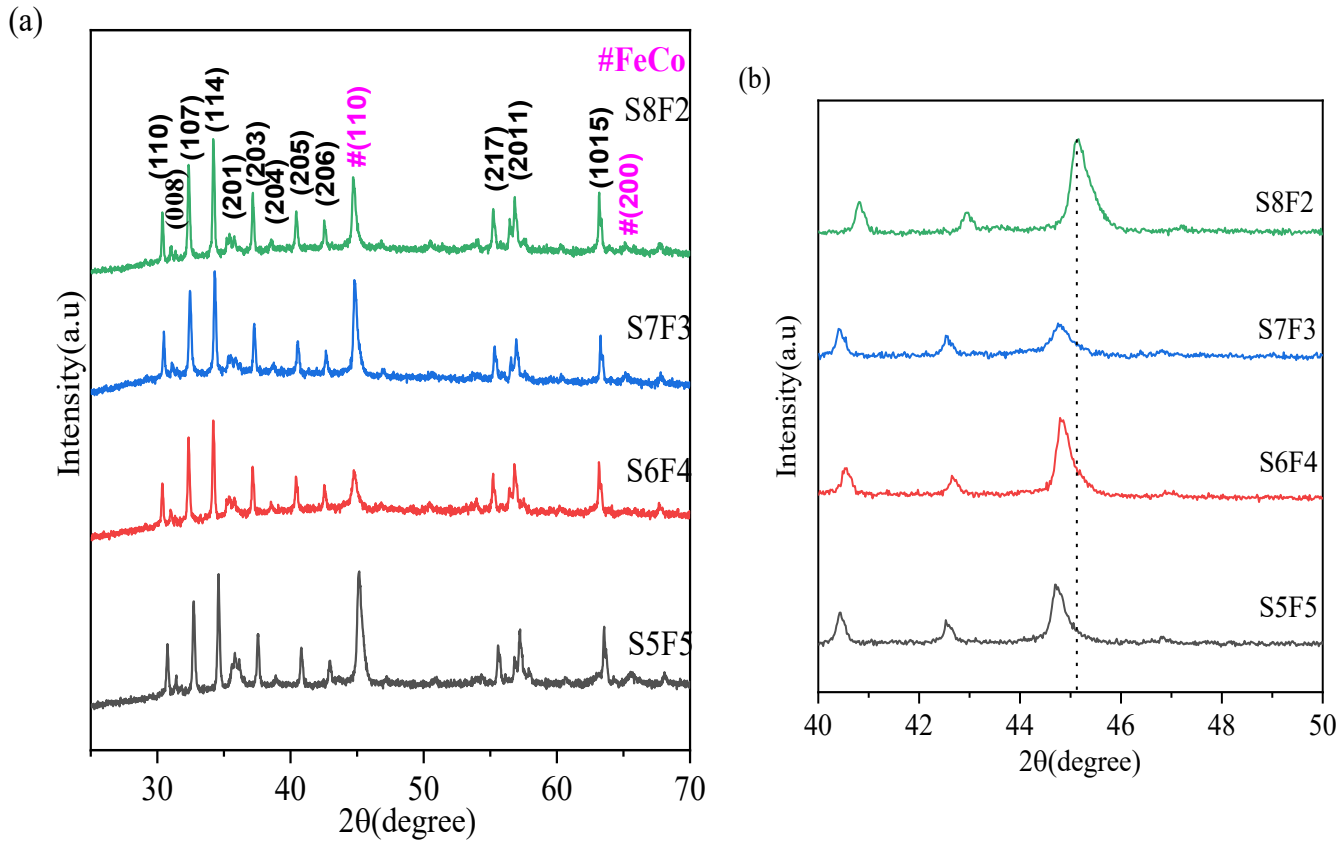

Figure 2. (a) XRD Patterns of $SrFe_{12}O_{19}$/FeCo nanocomposites for different ratios by physical mixing, **(b)** XRD Patterns of peak shift in $SrFe_{12}O_{19}$/FeCo nanocomposites.

Table 1. The structural parameters of the hard and soft phases $SrFe_{12}O_{19}$/FeCo for crystallite size for 4 different ratios.

$SrFe_{12}O_{19}$/ FeCo	D(nm) Soft	D(nm) Hard	Strain ($\varepsilon \times 10^{-3}$) Hard	Strain ($\varepsilon \times 10^{-3}$) Soft	Lattice parameters (Soft)	Lattice parameters (Hard)	
					a=b=c (Å)	a=b (Å)	c(Å)
S8F2	13	25	0.91	1.51	2.8417	5.780	22.981
S7F3	14	21	0.93	0.82	2.8532	5.884	23.979
S6F4	10	18	1.24	1.98	2.8624	5.875	22.978
S5F5	15	15	2.12	0.79	2.8634	5.880	23.976

The crystallite size of the FeCo soft phase decreases from 10 to 15 nm, while the $SrFe_{12}O_{19}$ hard phase decreases from 25 to 15 nm as the FeCo content increases. Among all the samples, the 60:40 composite shows the smallest FeCo crystalline size 10 nm. This reduction in crystallite size can be attributed to the strong interaction between the hard and soft phases, which limits the growth of FeCo crystallites during the synthesis process. Smaller FeCo crystallites provide a larger interfacial contact area with $SrFe_{12}O_{19}$, which is beneficial for improving the exchange interaction between the two magnetic phases [20]. The XRD pattern also shows that the FeCo (110) peak shifts slightly from about 45.1° to 44.7°in figure 2. According to Bragg's law, this leftward shift corresponds to an increase in the interplanar spacing (d-spacing), suggesting a slight expansion of the FeCo lattice distortion at the interface between $SrFe_{12}O_{19}$ and FeCo phases. [21] The 60:40 composite exhibits the highest FeCo strain (1.98×10^{-3}), which coincides with the smallest crystalline size. This indicates that a higher lattice strain restricts crystal growth and results in small crystalline size. In 50:50 composite shows a lower FeCo strain (0.79×10^{-3}) and a larger crystalline size (15 nm), suggesting that the lattice strain is decreasing, allowing the FeCo crystalline size increases. Meanwhile, the strain of the $SrFe_{12}O_{19}$ phase increases with increasing FeCo content, reaching 2.12×10^{-3} for the 50:50 composite, indicating increased interfacial stress in the hard phase. Overall, the reduction in crystalline size, the leftward shift of the FeCo (110) peak, and the increase in lattice strain confirm the presence of strong interfacial interaction between $SrFe_{12}O_{19}$ and FeCo, which is favorable for achieving partial exchange coupling in the nanocomposites. [22].

3.2 Morphological Studies

Figure 3 (a-d) shows the FESEM images of $SrFe_{12}O_{19}$/FeCo nanocomposites for different ratios. The FESEM images show two different types of particles present in the composites. Figure 3 (e) images of $SrFe_{12}O_{19}$/FeCo, show the presence of both the phases. Here, Figure 3 (a, b) images show hexagonal plates like morphology and agglomeration of quasi spherical like shape on the surface which confirms the presence of $SrFe_{12}O_{19}$ and FeCo particles. The image (c, d) the FeCo particles are agglomerated and widely spread on the surface of the $SrFe_{12}O_{19}$ particle Figure 4 the EDAX for S8F2 confirms the presence of $SrFe_{12}O_{19}$/FeCo where, Sr, Fe, Co and O are observed. No additional elements are observed which confirms the nanocomposites are free from impurities [23] Figure. 4(a-d) the elemental mapping for S8F2 shows the uniform distribution of Sr, Fe, Co confirms the presence of $SrFe_{12}O_{19}$ and FeCo phase. The Fe is uniformly distributed across the sample, while Co exhibits slight localization, shows the slight agglomeration of the FeCo phase. This suggests that although the composite shows overall mixing, the soft magnetic phase is not perfectly dispersed, which is characteristic of physical mixing. The coexistence of uniformly distributed ferrite and partially clustered FeCo phases confirms interfacial contact and confirms the partial exchange coupling.

3.3 High Resolution Transmission Electron Microscopy

Figure. 5 (a-c) shows the HRTEM images of sample d in 50nm, 100nm, 200nm respectively. Here, the images shows sharp, clear and hexagonal shape which reveals the high crystallinity being in accordance with the XRD results and confirms the hexagonal structure. And small quasi spherical on the surface of hexagonal shape confirms the formation of FeCo phase. This confirms the formation of composite between two phases. The fringe distance of about 0.202 nm and 0.216 nm are severally indexed to (110) and (114) planes of $SrFe_{12}O_{19}$ and FeCo. The SAED pattern (e) shows the crystallography and structural integrity of the material. The pattern exhibits well defined concentric rings of planes (307), (106), (206), (301) and (200) of $SrFe_{12}O_{19}$ hexagonal structure and FeCo BCC structure identified. Here, the presence of sharp diffraction spots from the larger grains confirms both the phases without any impurities. However, HRTEM was performed for one composition S8F2, the observed interface should not be interpreted as direct evidence of coupling across the entire composition series. Therefore, the conclusion of partial exchange coupling is based on the combined structural and magnetic characterization.

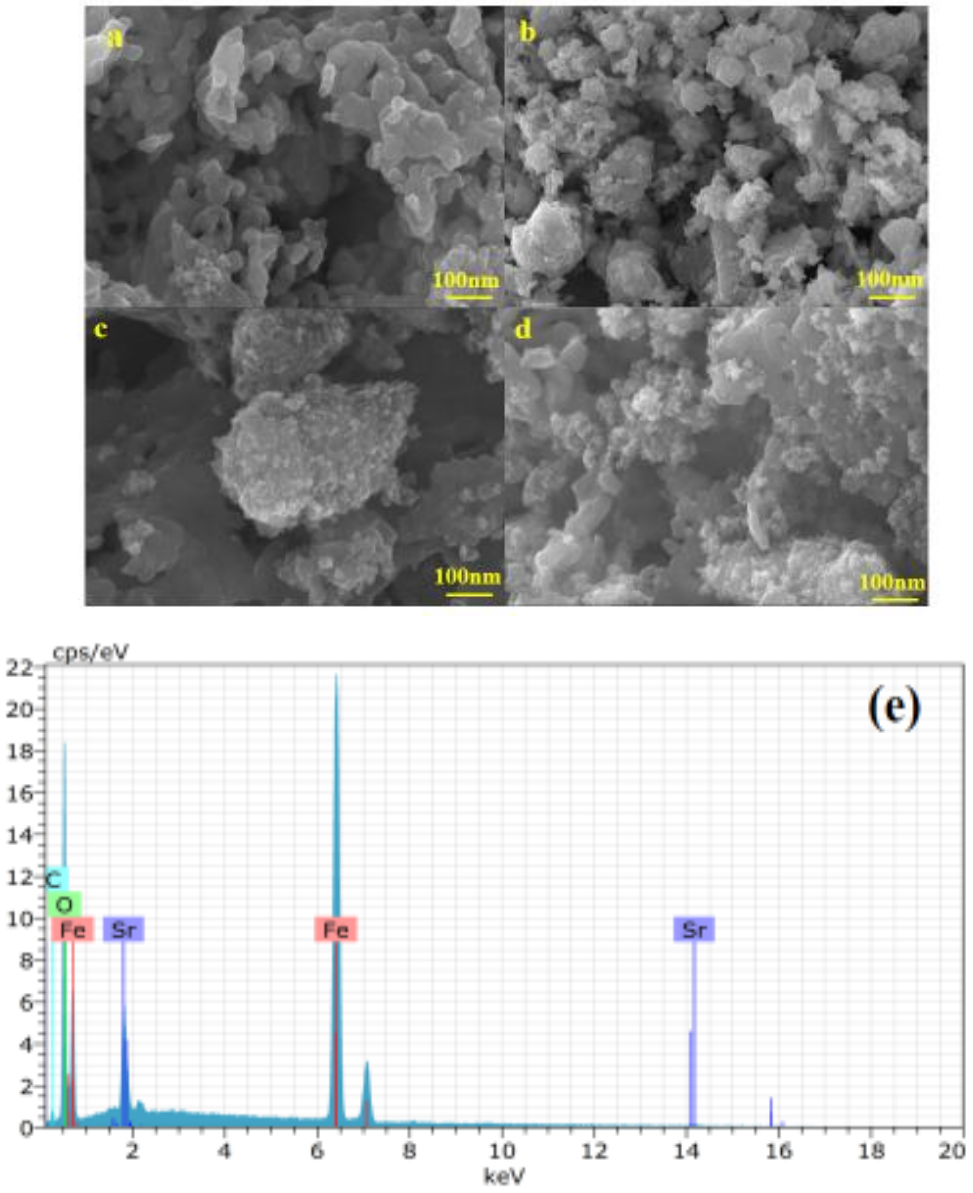

Figure 3. FESEM images of $SrFe_{12}O_{19}$/FeCo nanocomposites for different ratios, **(a)** S8F2 **(b)** S7F3 **(c)** S6F4 **(D)** S5F5, **(e)** Energy-dispersive X-ray spectroscopy for $SrFe_{12}O_{19}$/FeCo nanocomposite.

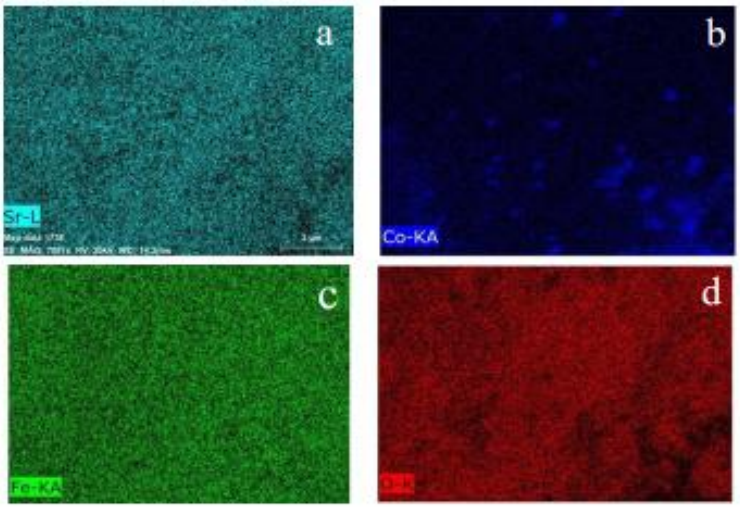

Figure 4. Elemental mapping of $SrFe_{12}O_{19}$/FeCo composite **(a)** sr **(b)** Co **(c)** Fe **(d)** O.

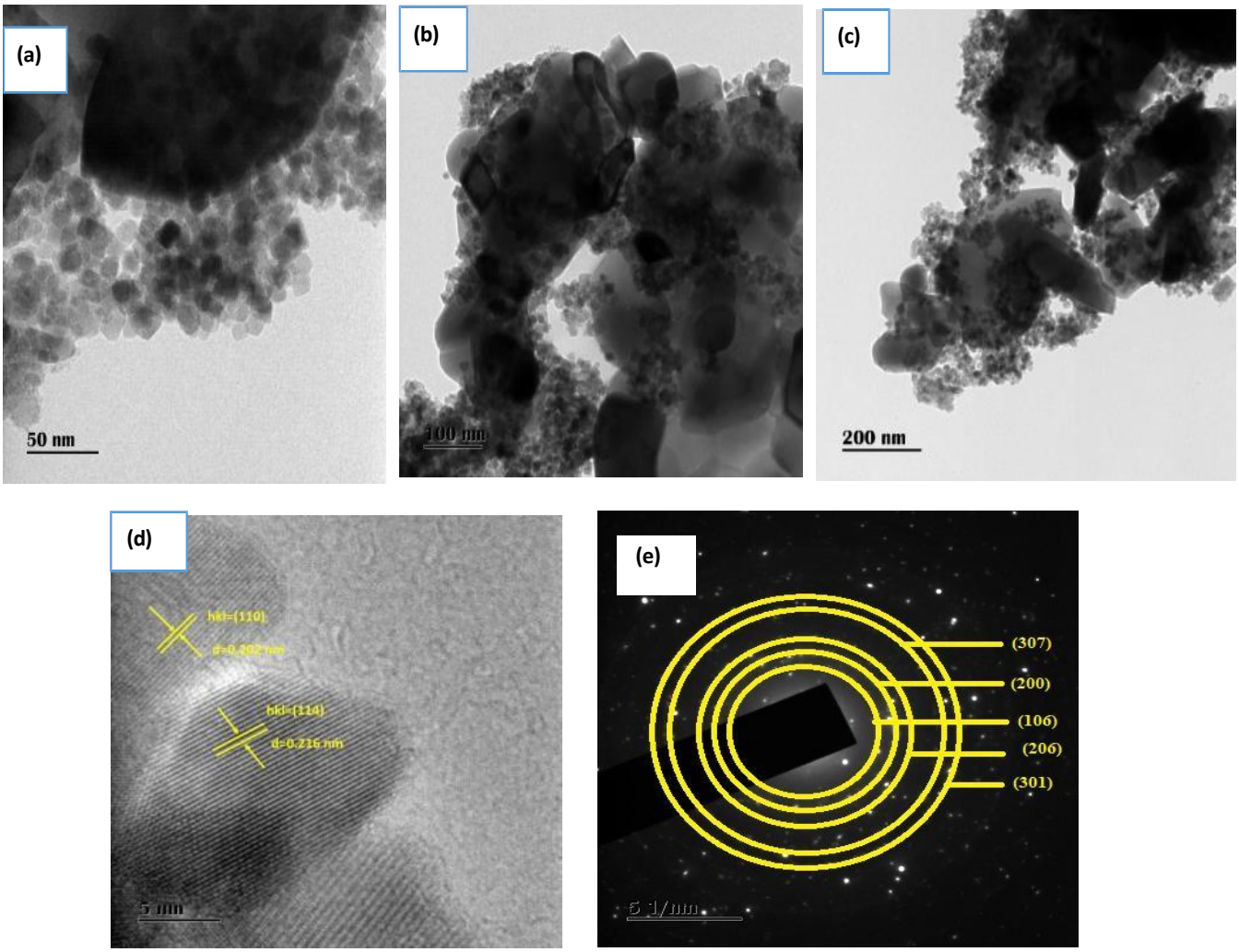

Figure 5. HRTEM images of $SrFe_{12}O_{19}$/FeCo nanocomposite for sample S_8F_2 **(a)** 50nm **(b)** 100nm **(c)** 200nm **(d)** SAED pattern **(e)** Orientation.

3.5 Vibrating Sample Magnetometer

Figure 6 shows the hysteresis loop of prepared samples which is carried out by VSM at room temperature with maximum applied field of 20000 Oe. The magnetic properties of the nanocomposites are influenced by the distribution of the hard and soft phases, the shape of the particles, the average grains size of the individual phases, the synthesis process, and the annealing temperatures. Here, $SrFe_{12}O_{19}$/FeCo nanocomposites for 4 different ratios are prepared i.e., $SrFe_{12}O_{19}$/FeCo [S8F2 (80:20), S7F3 (70:30), S6F4 (60:40), S5F5 (50:50)]. Here, the phase weight fractions and the resulting microstructural strain have a significant impact on the magnetic characteristics of the $SrFe_{12}O_{19}$/FeCo composites. The variation of magnetization saturation Ms, Coercivity (Hc), Remenence (Mr) are given in the Table 2.

The magnetic behavior of the $SrFe_{12}O_{19}$/ FeCo composites exhibits a strong dependence on composition and matches well with the structural features obtained from XRD analysis. When the ratio FeCo increased, the FeCo nanoparticles are agglomerated, and the hysteresis shows smooth loop with slight kink or shoulder which confirms the partial exchange coupling. [24] The saturation magnetization (M_s) values of samples S8F2 – S5F5 are 58, 53, 45 and 57 emu/g respectively. The S8F2 composite exhibits a high saturation magnetization of 58 emu/g, coercivity 1756 Oe, and remanent magnetization 18 emu/g because of the higher proportion of the hard magnetic $SrFe_{12}O_{19}$ phase, which results in large magnetocrystalline anisotropy and offers strong resistance to magnetization reversal. The crystallite size of $SrFe_{12}O_{19}$ for S8F2 is 25 nm and lattice strain is 0.91 × 10^{-3} indicates improved crystallinity with less lattice defects, resulting in stable magnetic domains and higher coercivity. In S7F3, coercivity reaches its maximum 1795 Oe shows that there is improved interaction between the phases and lattice strain values decreased for both the phases 0.82 × 10^{-3} and 0.93 × 10^{-3} shows less lattice distortion. In the S6F4, the saturation magnetization 45 emu/g, coercivity 949 Oe, and remanence 12 emu/g, although the FeCo crystallite size is reduced to 10 nm.

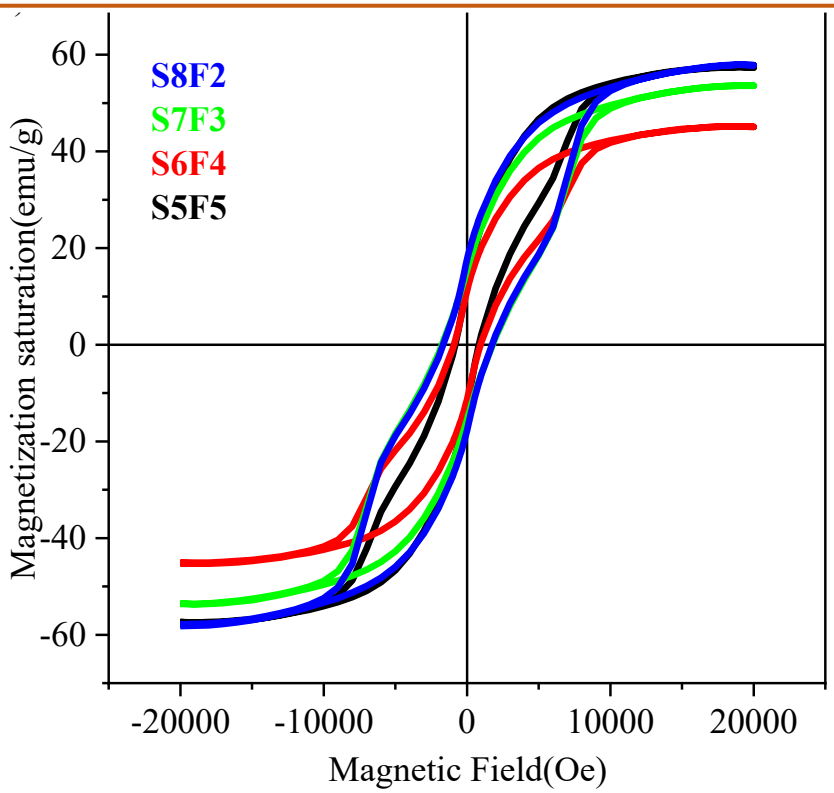

Figure 6. Hystersis loop of $SrFe_{12}O_{19}$/FeCo nanocomposites for different ratios by physical mixing.

Table 2. Saturation magnetization (M_s), Coercivity (H_c), Remenance (H_r) of $SrFe_{12}O_{19}$/FeCo Nanocomposite

Sample	Magnetization saturation M_s (emu/g)	Coercivity H_c (Oe)	Remenence M_r (emu/g)	M_r/M_s
S8F2	58	1756	18	0.31
S7F3	53	1795	15	0.28
S6F4	45	949	12	0.26
S5F5	57	866	11	0.19

This reduction is associated with the highest FeCo lattice strain 1.98 × 10^{-3} and the leftward shift of the FeCo (110) peak from 45.1° to 44.7°, indicating lattice expansion caused by interfacial stress between the FeCo phase and $SrFe_{12}O_{19}$ phase. The increased lattice strain shows residual stress and structural defects that disturb spin alignment and magnetic domain reversal, thereby reducing both the saturation magnetization and coercivity When the FeCo content is further increased to S5F5, the saturation magnetization increases again to 57 emu/g because FeCo possesses a much higher intrinsic magnetic moment than $SrFe_{12}O_{19}$. However, the coercivity 866 Oe and remanence 11 emu/g decrease further because the increasing fraction of the soft magnetic FeCo phase lowers the overall magnetocrystalline anisotropy and allows easier magnetization reversal. The increase in FeCo crystallite size 15 nm together with the decrease in FeCo lattice strain 0.79 × 10^{-3} indicates partial relaxation of internal stress and grain growth, whereas the $SrFe_{12}O_{19}$ phase exhibits the highest strain 2.12 × 10^{-3}, confirming increased interfacial stress in the hard phase. [25, 26] The XRD values of crystallite size, lattice strain, and peak shift strongly influence the magnetic behavior of the composites.

Squareness of hard/soft nanocomposites is one of the important determining factors on the exchange coupling interactions. According to the stoner-wohlforth theory, for hard/soft nanocomposites M_r/M_s ratio above 0.5% which confirms the exchange coupling interactions. Meanwhile, the squareness values of sample S8F2 to S5F5 from between 0.31 to 0.19 shows the pinning capability of the hard phase controls the magnetization process, these mechanically mixed composites could not attain a fully developed exchange coupling [27]. These results shows that interfacial interactions and domain dynamics, rather of intrinsic structural changes, control magnetic behaviour. For analyzing more, derivation of magnetization data concerning the external magnetic field (dM/dH) is done.

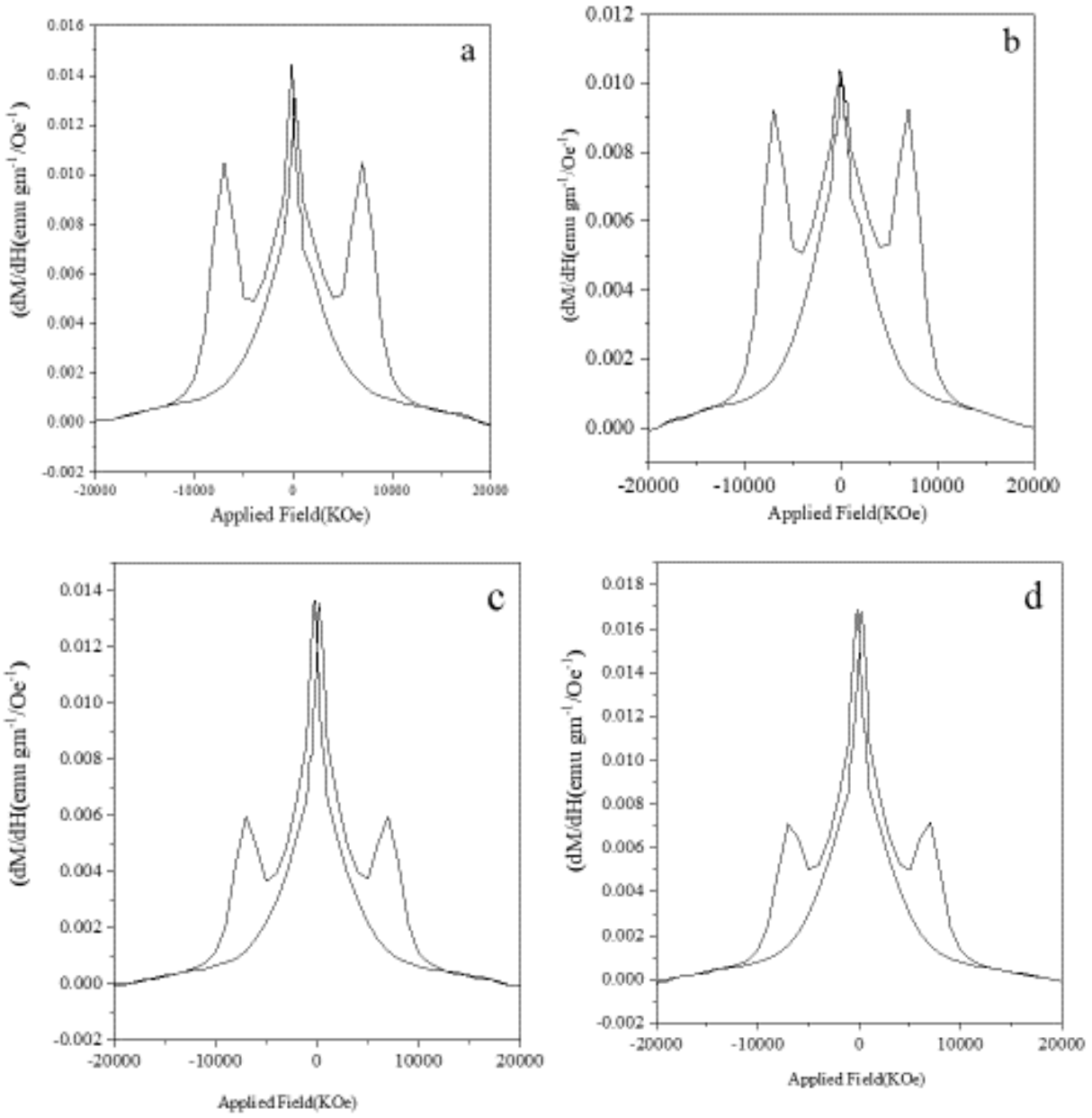

Figure 7. dM/dH vs H plotes performed at room temperature for prepared 4 different ratio **(a)** S8F2 (b0 S7F3 **(c)** S6F4 **(d)** S5F5.

Table 3. Maximum Energy product and Magneto crystalline anisotropy of $SrFe_{12}O_{19}$/FeCo nanocomposite.

Sample	BH_{Max} (MGOe)	Magneto crystalline anisotropy ×104 J/m^{-3}
S8F2	0.18	2.82
S7F3	0.17	2.63
S6F4	0.10	1.18
S5F5	0.09	1.36

The dM/dH curves (figure 7a – 7d) of the $SrFe_{12}O_{19}$/FeCo nanocomposites (S8F2, S7F3, S6F4, S5F5) shows magnetization reversal behavior and switching field distribution (SFD) of the hard-soft magnetic phases. All four samples exhibit a sharp central peak near zero applied field by two symmetric secondary peaks at higher positive and negative fields. The sharp central peak indicates the collective magnetization reversal of the exchange-coupled $SrFe_{12}O_{19}$ and FeCo phases, whereas the secondary peaks correspond to independently reversing FeCo phase that are partially coupled or magnetically separated from the hard ferrite phase with strong interaction.

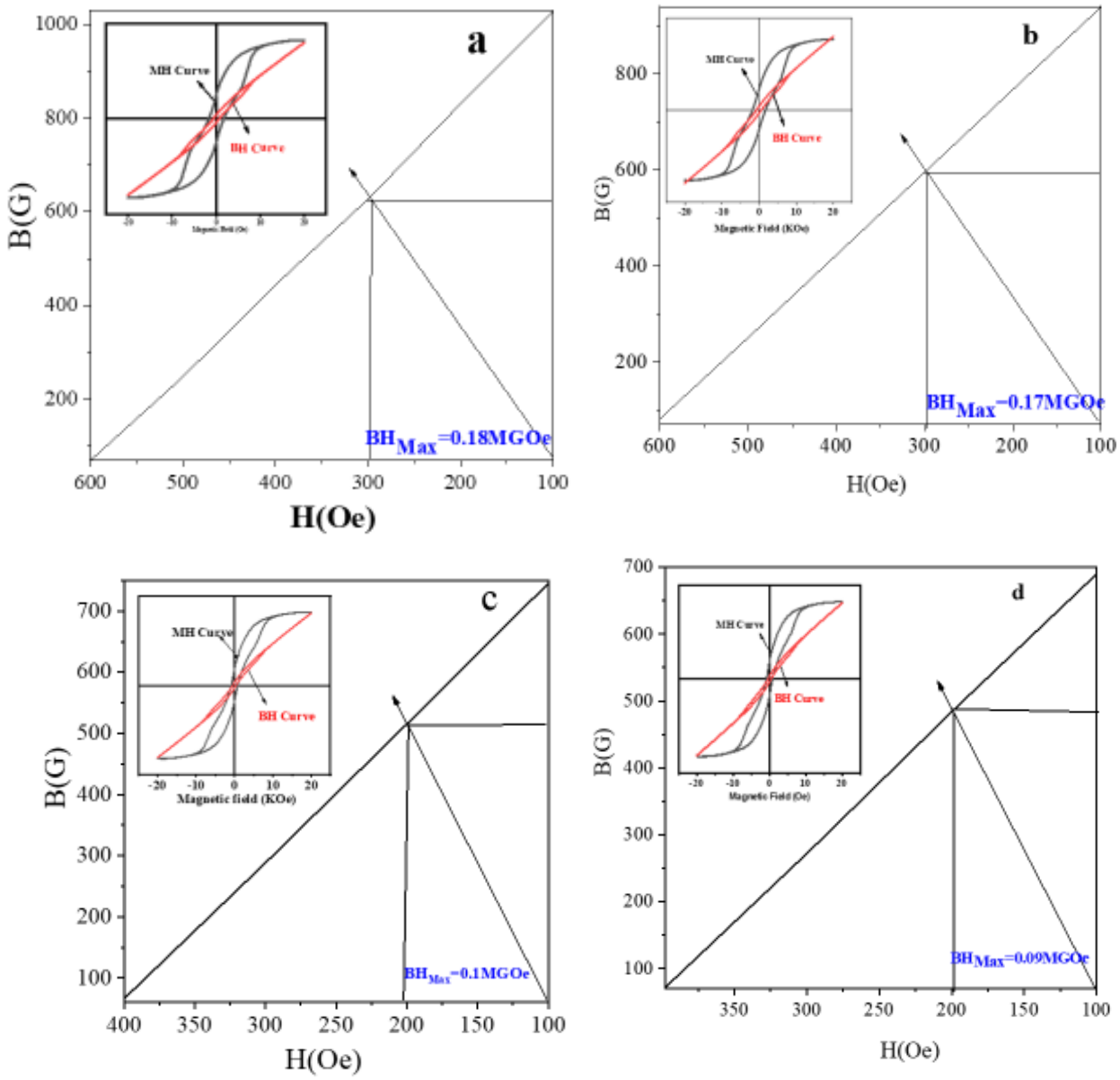

Figure 8. Maximum energy product for prepared 4 samples of different ratio, **(a)** S8F2, **(b)** S7F3, **(C)** S6F4, **(d)** S5F5.

The presence of these multiple switching events confirms that the composites exhibit partial exchange coupling rather than ideal exchange-spring behavior, suggesting that only a fraction of the FeCo particles are effectively exchange-coupled with $SrFe_{12}O_{19}$, while the remaining particles reverse independently due to non-uniform particle distribution, agglomeration. Among the four compositions, the S5F5 sample shows the highest central peak intensity, indicating stronger interfacial exchange interaction and enhanced cooperative magnetization reversal, whereas S7F3 exhibits a relatively broader and less intense central peak, reflecting a wider switching field distribution and greater magnetic heterogeneity. The S8F2 and S6F4 samples display intermediate behavior with pronounced central peaks and visible side peaks, demonstrating that exchange interactions are present but remain incomplete.

These dM/dH curves are directly related to the remanence Mr values. A strong and sharp central peak indicates that most of the $SrFe_{12}O_{19}$and FeCo particles reverse together because of effective exchange coupling. As a result, more magnetic moments remain aligned after the external magnetic field is removed, leading to higher remanence. In contrast, broader central peaks and more prominent side peaks indicate that some FeCo particles reverse independently from the hard $SrFe_{12}O_{19}$ phase. These weakly coupled regions lose their magnetic alignment more easily after the field is removed, resulting in lower remanence. According to this the higher remanence observed for S8F2 and S5F5 is consistent with their stronger central dM/dH peaks, while the lower remanence of S7F3 and S6F4 is associated with broader switching field distributions and a larger contribution from independently reversing FeCo regions. Therefore, the

dM/dH analysis confirms that the remanence of the $SrFe_{12}O_{19}$/FeCo nanocomposites depends on the strength of the exchange coupling and the fraction of magnetic particles that reverse collectively [28, 8, 21, -23]. This behavior is shows that $SrFe_{12}O_{19}$/FeCo of partially exchange-coupled hard-soft magnetic nanocomposites with strong interaction.

Here, magnetocrytalline anisotropy is the fundamental magnetic property that describes the dependence of magnetization direction on the crystal structure of a material. The magnetocrystalline anisotropy of the composite $SrFe_{12}O_{19}$/FeCo is calculated by,

$$K = \frac{\mu 0.Hc.Ms}{2} \quad (3)$$

Where, K is the effective magnetocrystalline anisotropy constant (J m^{-3}), μ0 is the permeability of free space ($4\pi \times 10^{-7}$ H m^{-1}), Hc is the coercivity (A m^{-1}), and Ms is the saturation magnetization (A m^{-1}). The calculated values are listed in table 3.

The increase in magnetocrystalline anisotropy (K) and maximum energy product BHmax with composition (figure 8) shows a considerable dependence on interfacial interactions and phase balance in ferrite alloy composites. The significant decrease in K from 2.82× 10^4 to 1.36 × 10^4 J/m^3 is directly correlated with the with lattice strain observed in the XRD. [24, 27] The hexaferrite matrix induces stress-induced anisotropy, which enhances the effective magnetocrystalline energy of the hexagonal structure. Similarly the increase in BHmax improves magnetic energy storage relation between magnetization and coercivity. Even though it is physical mixed the particles contact with higher alloy content gives strong interaction between the phases. The three distinct peaks of $SrFe_{12}O_{19}$/FeCo composite with partial exchange coupling maintains the balance between magnetization and coercivity which maximum energy product with tunable switching field distribution.

4. Conclusion

In this study, $SrFe_{12}O_{19}$/FeCo hard–soft magnetic nanocomposites with four different phase ratios were successfully prepared using a simple physical mixing method. The XRD results confirmed the coexistence of the hexagonal $SrFe_{12}O_{19}$ hard magnetic phase and the body-centred cubic FeCo soft magnetic phase, with no detectable impurity peaks. The morphology, elemental composition, and elemental distribution were further investigated using FESEM and HRTEM for the sample exhibiting the highest saturation magnetization. The magnetic properties of all four compositions were evaluated using VSM, and the results demonstrated that the magnetic behaviour strongly depends on the $SrFe_{12}O_{19}$/FeCo ratio. The combination of the hard $SrFe_{12}O_{19}$ phase with the high-magnetization FeCo soft phase effectively modified the overall magnetic properties of the composites. In particular, the maximum energy product (BH) max increased from 0.09 to 0.18 MGOe, indicating that an appropriate hard-to-soft phase ratio can improve the energy-producing capability of the material. The physical mixing method offers important advantages, including a simple preparation process, low cost, and ease of controlling the composition compared with more complex synthesis methods. Moreover, this approach allows the hard and soft magnetic phases to interact while largely retaining their individual magnetic characteristics. Overall, the results demonstrate that physically mixed $SrFe_{12}O_{19}$/FeCo nanocomposites have good potential as rare-earth-free permanent magnetic materials. Further optimization of the phase ratio, particle size, and interfacial interaction between the hard and soft phases could provide additional improvements in their magnetic performance and energy product, supporting their potential use in permanent magnet applications.

References

[1] C. Sirisathitkul, Y. Sirisathitkul, Recent developments in 3D printing of rare-earth-free permanent magnets. Inventions, 7(3), (2022) 71. https://doi.org/10.3390/inventions7030071

[2] A. Bollero, J. Rial, M. Villanueva, K.M. Golasinski, A. Seoane, J. Almunia, R. Altimira, Recycling of strontium ferrite waste in a permanent magnet manufacturing plant. ACS Sustainable Chemistry & Engineering, 5(4), (2017) 3243-3249. https://doi.org/10.1021/acssuschemeng.6b03053

[3] J.N. Dahal, D. Neupane, T.P. Poudel, Synthesis and magnetic properties of 4:1 hard-soft $SrFe_{12}O_{19}$-$Lr_{1-x}Sr_xMnO_3$ nanocomposite prepared by autocombustion method, AIP Advances, 9(7), (2019) 075308. https://doi.org/10.1063/1.5096530

[4] M.I. Mørch, J.V. Ahlburg, M. Saura-Múzquiz, A.Z. Eikeland, M. Christensen, Structure and magnetic properties of W-type hexaferrites. IUCrJ, 6(3), (2019) 492-499. https://doi.org/10.1107/S2052252519003130

[5] C. de Julián Fernández, C. Sangregorio, J. de la Figuera, B. Belec, D. Makovec A. Quesada, Progress and prospects of hard hexaferrites for permanent magnet applications, Journal of Physics D: Applied Physics, 54, (2021) 153001. https://doi.org/10.1088/1361-6463/abd272

[6] E. Kiani, A.S. Rozatian, M.H. Yousefi, Synthesis and characterization of $SrFe_{12}O_{19}$ nanoparticles produced by a low-temperature solid-state reaction method. Journal of Materials Science: Materials in Electronics, 24(7), (2013) 2485-2492. https://doi.org/10.1007/s10854-013-1122-5

[7] Y. Qie, Y. Liu, F. Kong, Z. Yang, H. Yang, Exchange-coupling of hard/soft magnetic phases of Co/FeCo nanocomposites. The Journal of Physical Chemistry C, 126(20), (2022) 8826-8831. https://doi.org/10.1021/acs.jpcc.2c00457

[8] C. Granados-Miralles, A. Quesada, M. Saura-Múzquiz, H.L. Andersen, J.F. Fernández, M. Christensen, Expanding the tunability and applicability of exchange-coupled/decoupled magnetic nanocomposites. Materials Chemistry Frontiers, 4(4), (2020) 1222-1230. https://doi.org/10.1039/c9qm00713j

[9] D. Lisjak, M. Drofenik, Chemical Substitution an Alternative Strategy for Controlling the Particle Size of Barium Ferrite. Crystal growth & design, 12(11), (2012) 5174-5179. https://doi.org/10.1021/cg301227r

[10] W. Zhong, W. Ding, N. Zhang, J. Hong, Q. Yan, Y. Du, Key step in synthesis of ultrafine $BaFe_{12}O_{19}$ by sol-gel technique. Journal of Magnetism and Magnetic Materials, 168(1-2), (1997) 196-202. https://doi.org/10.1016/S0304-8853(96)00664-6

[11] W. Roos, Formation of chemically coprecipitated barium ferrite. Journal of the American Ceramic Society, 63(11-12), (1980) 601-603. https://doi.org/10.1111/j.1151-2916.1980.tb09843.x

[12] D. Lisjak, M. Drofenik, The mechanism of the low-temperature formation of barium hexaferrite. Journal of the European Ceramic Society, 27(16), (2007) 4515-4520. https://doi.org/10.1016/j.jeurceramsoc.2007.02.202

[13] S. Dudziak, Z. Ry˙zynska, Z. Bielan,a J. Ryl, T. Klimczuk, A.Z. Jurek, Pseudo-superparamagnetic behaviour of barium hexaferrite particles. RSC Advances, 10(32), (2020) 18784-18796. https://doi.org/10.1039/d0ra01619e

[14] J. Ding, W.F. Miao, P.G. McCormick, R. Street, High-coercivity ferrite magnets prepared by mechanical alloying. Journal of Alloys and Compounds, 281(1), (1998) 32–36. https://doi.org/10.1016/S0925-8388(98)00766-X

[15] F.N. Tenorio-González, A.M. Bolarín-Miró, F. Sánchez-De Jesús, P. Vera-Serna, N. Menéndez-González, J. Sánchez-Marco, Crystal structure and magnetic properties of high Mn-doped strontium hexaferrite. Journal of Alloys and Compounds, 695, (2017) 2083-2090. https://doi.org/10.1016/j.jallcom.2016.11.047

[16] V. Pillai, P. Kumar, D.O. Shah, Magnetic properties of barium ferrite synthesized using a microemulsion mediated process. Journal of Magnetism and Magnetic Materials, 116(3), (1992) L299-L304. https://doi.org/10.1016/0304-8853(92)90105-W

[17] T. Gonzalez-Carreno, M.P. Morales, C.J. Serna, Barium ferrite nanoparticles prepared directly by aerosol pyrolysis. Materials Letters, 43(3), (2000) 97–101. https://doi.org/10.1016/S0167-577X(99)00238-4

[18] K.S. Martirosyana, E. Galstyan, S.M. Hossain, Yi-Ju Wangc, D. Litvinova, Barium hexaferrite nanoparticles: Synthesis and magnetic properties. Materials Science and Engineering: B, 176(1), (2011) 8–13. https://doi.org/10.1016/j.mseb.2010.08.005

[19] L. Rezlescu, E. Rezlescu, P.D. Popa, N. Rezlescu, Fine barium hexaferrite powder prepared by the crystallisation of glass. Journal of Magnetism and Magnetic Materials, 193(1-3), (1999) 288-290. https://doi.org/10.1016/S0304-8853(98)00442-9

[20] R. Müller, R. Hiergeist, H. Steinmetz, N. Ayoub, M. Fujisaki, W. Schüppel, Barium hexaferrite ferrofluids preparation and physical properties. Journal of Magnetism and Magnetic Materials, 201(1-3), (1999) 34-37. https://doi.org/10.1016/S0304-8853(99)00016-5

[21] D. Barb, L. Diamandescu, A. Rusi, D. Tarabasanu-Mihaila, M. Morariu, V. Teodorescu, Preparation of barium hexaferrite by a hydrothermal method: structure and magnetic properties. Journal of materials science, 21(4), (1986) 1118-1122. https://doi.org/10.1007/BF00553240

[22] L. Pan, D. Cao, P. Jing, J. Wang, Q. Liu, A novel method to fabricate $CoFe_2O_4/SrFe_{12}O_{19}$ composite ferrite nanofibers with enhanced exchange coupling effect. Nanoscale Research Letters, 10(1), (2015) 131. https://doi.org/10.1186/s11671-015-0829-z

[23] D.R. Sahoo, A. Barik, R. Ghosh, S. Mishra, J. Ray, S. Kuila, P. Vishwakarma, Investigation of structural of structural changes in bismuth substituted SrFe12O19 compound using in-situ raman spectroscopy. Journal of Condensed matter. World Science Publications, 2(02), (2025) 110-113. https://doi.org/10.61343/jcm.v2i02.109

[24] F. Liu, y. hou, S. Gao, Exchange-coupled nanocomposites: chemical synthesis, characterization and applications. Chemical Society Reviews, 43, (2014) 8098-8113. https://doi.org/10.1039/c4cs00162a

[25] P. Jing, J. Du, J. Wang, J. wei, L. Pan, J. Li, Q. Liu, Width-controlled M-type hexagonal strontium ferrite ($SrFe_{12}O_{19}$) nanoribbons with high saturation magnetization and superior coercivity synthesized by electrospinning. Scientific Reports, 5(1), (2015) 15089. https://doi.org/10.1038/srep15089

[26] S.M. Taimoory, J.F. Trant, A. Rahdar, M. Aliahmad, F. Sadeghfar, M. Hashemzaei, Importance of the inter-electrode distance for the electrochemical synthesis of magnetite

nanoparticles: synthesis, characterization, computational modelling, and cytotoxicity. E-Journal of Surface Science and Nanotechnology, 15, (2017) 31-39. https://doi.org/10.1380/ejssnt.2017.31

[27] E.F. Kneller, R. Hawig, The exchange-spring magnet: a new material principle for permanent magnets. IEEE Transactions on Magnetics, 27(4), (1991) 3588-3560. https://doi.org/10.1109/20.102931

[28] S. Torkian, A. Ghasemi, R.S. Razavi, Magnetic properties of hard-soft $SrFe_{10}Al_2O_{19}/Co_{0.8}Ni_{0.2}Fe_2O_4$ ferrite synthesized by one-pot sol–gel auto combustion. Journal of Magnetism and Magnetic Materials, 416, (2016) 408-416. https://doi.org/10.1016/j.jmmm.2016.05.050

Authors Contribution Statement

R. Akshaya: Conceptualization, Formal analysis, Investigation, Visualization, Writing-original draft. B. Gokul: Conceptualization, Supervision, Validation, Writing-review & editing. Both authors reviewed and approved the final version of the manuscript.

Funding

The authors declare that no funds, grants or any other support were received during the preparation of this manuscript.

Competing Interests

The authors declare that there are no conflicts of interest regarding the publication of this manuscript.

Data Availability

The data supporting the findings of this study can be obtained from the corresponding author upon reasonable request.

Has this article screened for similarity?

Yes

About the License